‡Electronic Supplementary Information (ESI):

Supplementary Figures and Tables

Optogenetic modulation of real-time nanoscale dynamics of HCN channels using photoactivated adenylyl cyclases

Meenakshi Tanwar, Suneel Kateriya, Deepak Nair, Mini Jose

Table of Contents

A)

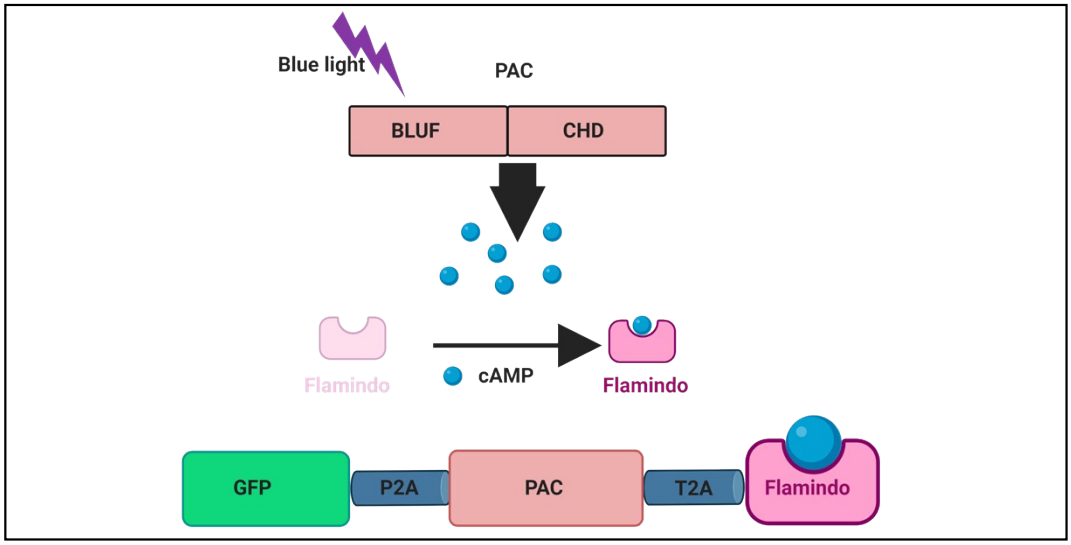

B)

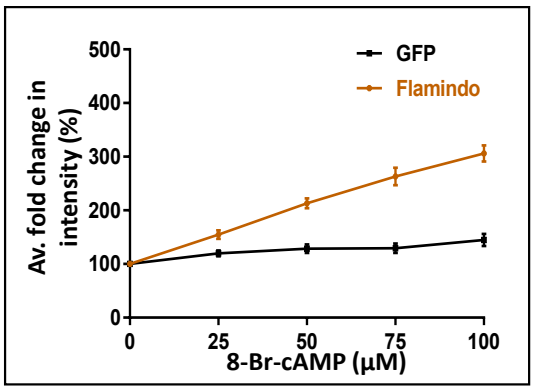

C)

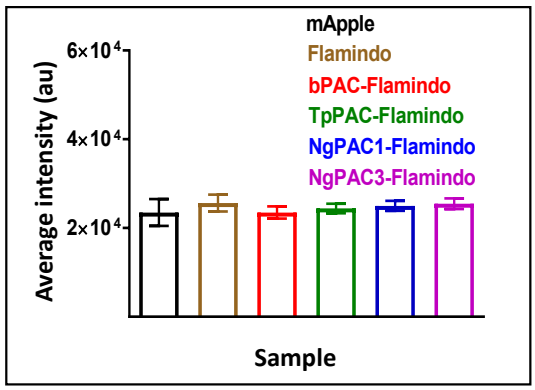

D)

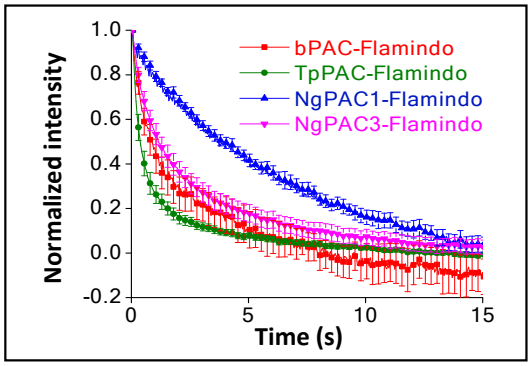

E)

Construct	A1	τ_1 (s)	A2	τ_2 (s)	τ_{av} (s)
bPAC-Flamindo	1.71	0.50	1.23	3.39	1.71
TpPAC-Flamindo	1.08	0.33	0.33	5.05	1.43
NgPAC1-Flamindo	0.57	3.78	0.91	19.32	13.32
NgPAC3-Flamindo	1.68	0.65	1.36	4.20	2.24

Figure S1. **Photophysical characterization of the PAC variants. A)** A scheme representing the photoactivated adenylyl cyclase protein which synthesizes cAMP upon photoactivation, Flamindo sensor whose fluorescence increases upon binding to cAMP and the constructs used for co-expression of PAC and Flamindo. P2A and T2A represent self-cleaving sites (ESI‡). **B)** Dose-response curve of Flamindo sensor and GFP with increasing concentration of cAMP. In contrast to GFP, Flamindo displayed a significant increase in average fold change in intensity with increasing intracellular cAMP levels. **C)** Average intensity of GFP::PAC in cells assessed for intensity changes of Flamindo by photoactivation as shown in Fig. 1C, where mApple and Flamindo denote controls. **D)** Temporal changes in fluorescence intensity of Flamindo upon targeted photoactivation of PACs (bPAC, TpPAC, NgPAC1, and NgPAC3) using a 488 nm laser (n=9, error bars indicate s.e.m from 2 biological replicates). **E)** Table illustrates the biophysical properties of fluorescence decay from D.

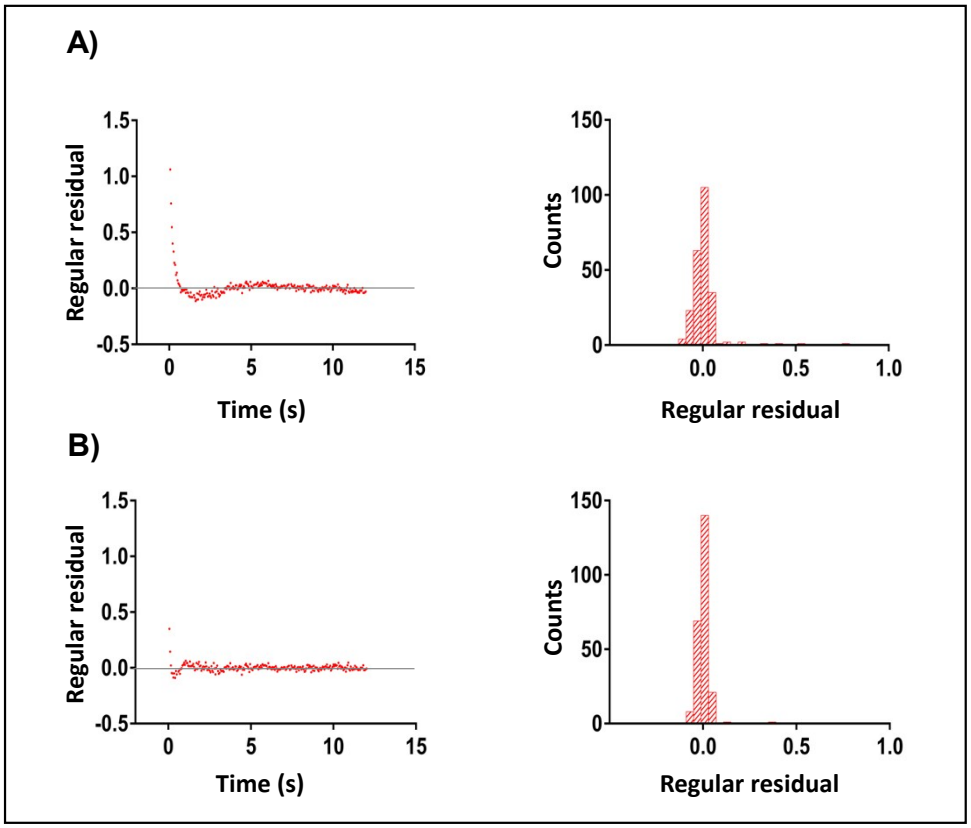

Figure S2. Comparative plots of the fluorescence decay fit by single and bi-exponential models. Left panel) The fluorescence decay of a cell expressing bPAC-Flamindo was fit by single **(A)** and bi-exponential **(B)** models. **Right panel)** Comparative plots of the measured residues as a function of time for the two models are shown. The fit was significantly better using a bi-exponential model compared to the single.

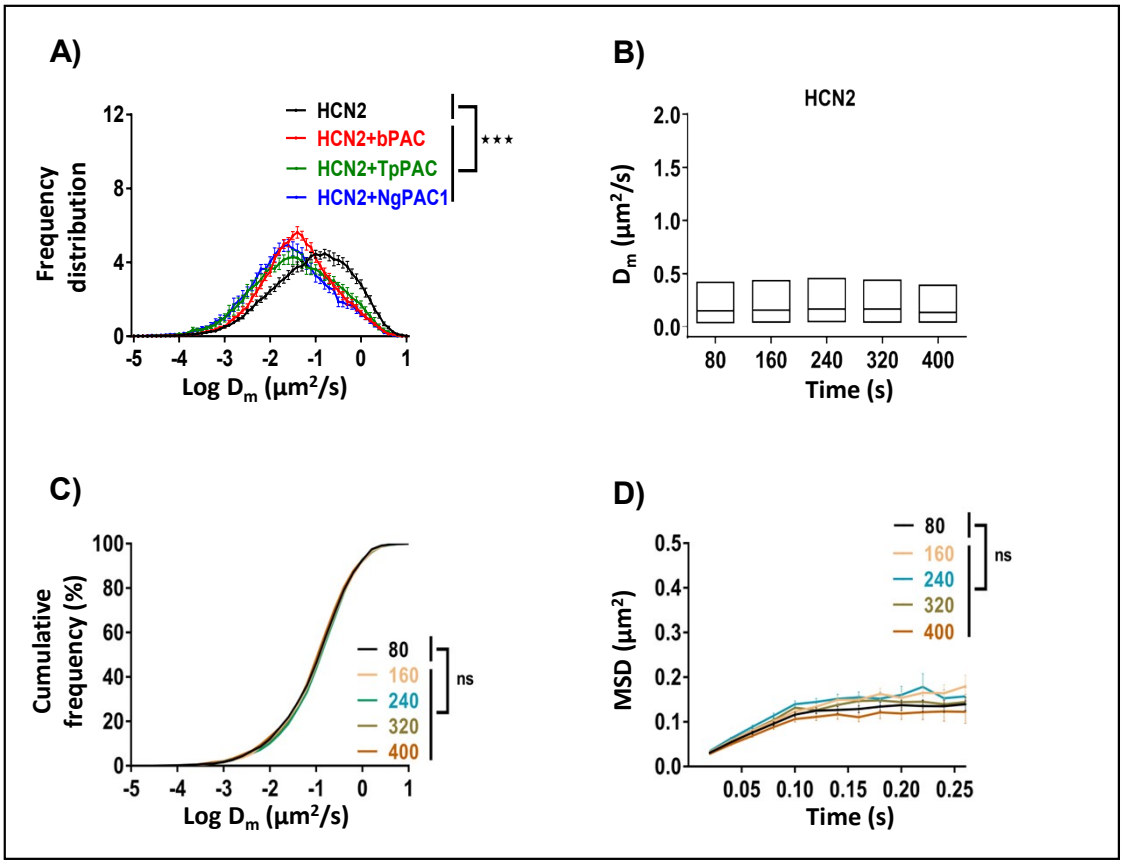

Figure S3. Time dependent mobility characteristics of mEos::HCN2 in live cells. A) Comparative frequency distribution of mEos::HCN2 molecules which displayed reduced mobility upon light regulated elevation of cAMP level by acute photoactivation of PACs (n=10, mean± s.e.m from 2 biological replicates, ***p<0.001, 2-way Anova). **B)** Diffusion coefficient (D_m) of control mEos::HCN2 which remained unaltered for five subsequent time windows corresponding to 80s, 160s, 240s, 320s and 400s during continuous exposure of 405 nm at low intensities. **C, D)** Time dependent cumulative distribution of instantaneous diffusion coefficient and MSD curve of control mEos::HCN2 which did not display any significant alterations during continuous exposure of 405 nm at low intensities (2-way Anova). ns-not significant.

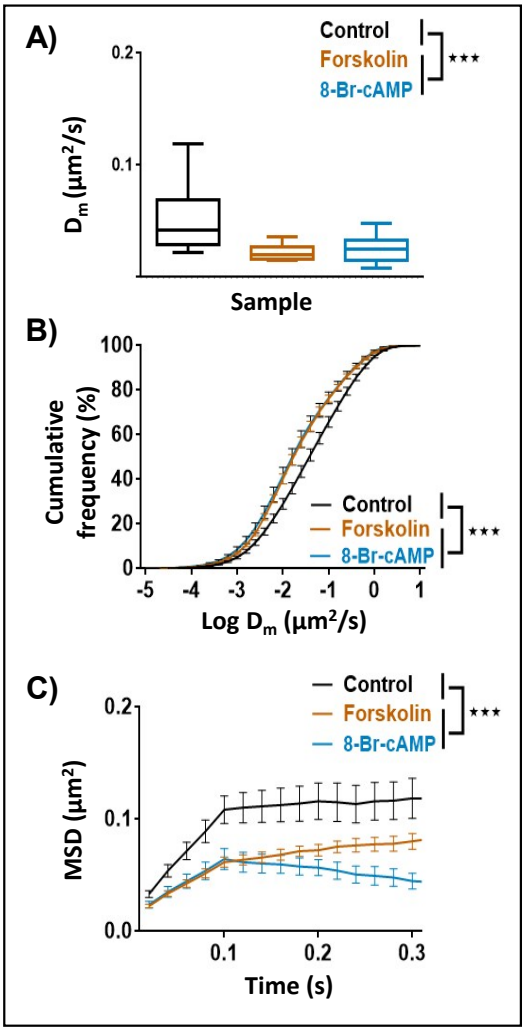

Figure S4. Comparative diffusion dynamics of mEos::HCN2 after pharmacological modulation of cAMP in live cells. A) Comparison of average diffusion coefficient of mEos::HCN2 before and after forskolin or 8-Br-cAMP application (n=7, median/IQR, ***p<0.001, Mann-Whitney test). **B, C)** Cumulative frequency distribution of instantaneous diffusion coefficients and MSD curve of mEos::HCN2 before and after forskolin or 8-Br-cAMP application, respectively (n=7, mean± s.e.m from 2 biological replicates, ***p<0.001, 2-way Anova). The mobility of mEos::HCN2 was significantly reduced on elevating intracellular cAMP levels by forskolin or by application of 8-Br-cAMP.

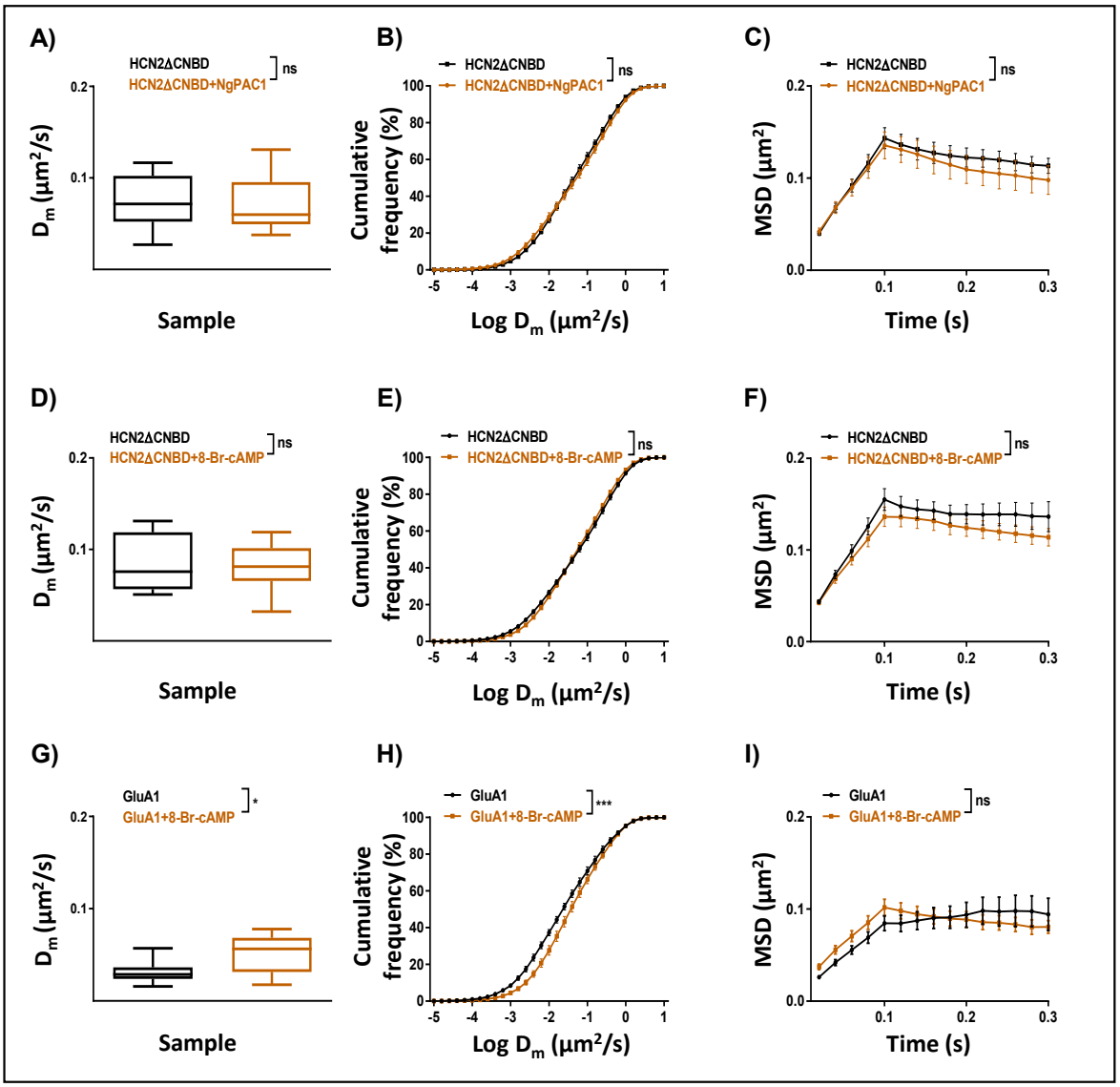

Figure S5. Comparative diffusion dynamics of mEos::HCN2ΔCNBD and GluA1::mEos upon cAMP modulation in live cells. A-C) Diffusion dynamics of mEos::HCN2ΔCNBD upon optogenetic modulation of cAMP in live cells. **A)** Comparison of the average diffusion coefficient of mEos::HCN2ΔCNBD before and after increasing the cAMP level by photoactivation of NgPAC1 (n=8, median/IQR, Mann-Whitney test). **B, C**) Cumulative frequency distribution of instantaneous diffusion coefficient and MSD curve of mEos::HCN2ΔCNBD before and after elevation of cAMP level via photoactivation of NgPAC1, respectively (n=8, 2-way Anova). **D-F)** Comparative diffusion dynamics of mEos::HCN2ΔCNBD after pharmacological modulation of cAMP in live cells. **D)** Comparison of average diffusion coefficient of mEos::HCN2ΔCNBD before and after 8-Br-cAMP application (n=9, median/IQR, Mann-Whitney test). **E, F)** Cumulative frequency distribution of instantaneous diffusion coefficient and MSD curve of mEos::HCN2ΔCNBD before and after 8-Br-cAMP application, respectively (n=9, 2-way Anova). **G-I)** Diffusion dynamics of GluA1::mEos after pharmacological modulation of cAMP in live cells. **G)** Average diffusion coefficient of GluA1::mEos before and after 8-Br-cAMP application (n=9, median/IQR, *p<0.05, Mann-Whitney test). **H, I)** Cumulative frequency distribution of instantaneous diffusion coefficient and MSD plot of GluA1::mEos before and after 8-Br-cAMP application, respectively (n=9, 2-way Anova). All cumulative frequency and MSD graphs display mean± s.e.m from 2 biological replicates. Diffusion dynamics of mEos::HCN2ΔCNBD remained unaltered in presence of cAMP in contrast to GluA1::mEos which displayed a slight increase in mobility. ns-not significant.

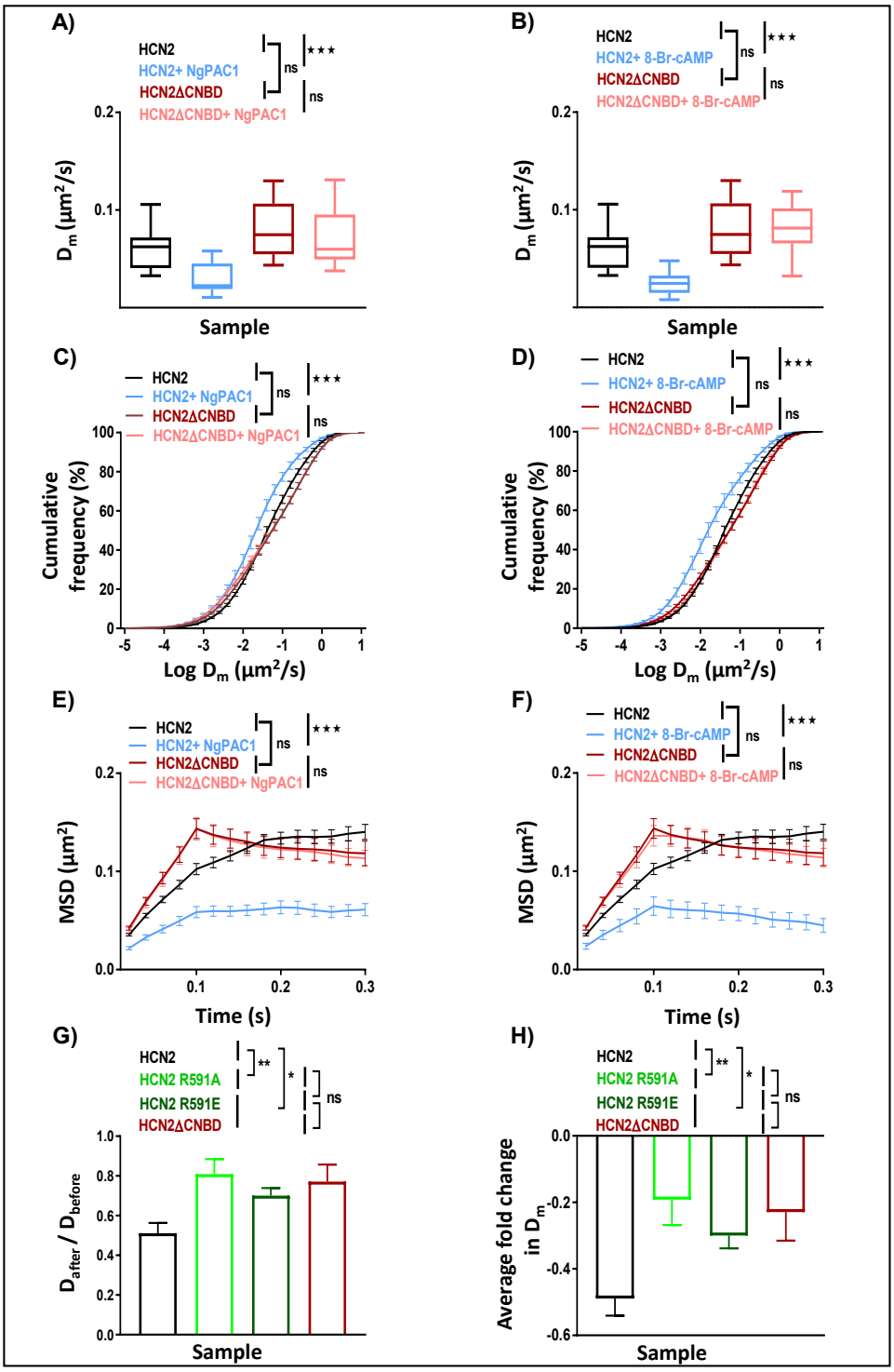

Figure S6. Comparative analysis of mobility kinetics of HCN2, its deletion construct lacking CNBD and HCN2 point mutants upon stimulation. A, B) Comparison of average diffusion coefficient of wild type mEos::HCN2 and mEos::HCN2ΔCNBD upon optical and pharmacological stimulation, respectively (n=16, median/IQR, ***p<0.001, Mann-Whitney test). **C, D)** Cumulative frequency distribution of instantaneous diffusion coefficient of mEos::HCN2 and mEos::HCN2ΔCNBD upon optical and pharmacological stimulation, respectively (n=16, mean± s.e.m from 2 biological replicates, ***p<0.001, 2-way Anova). **E, F)** MSD curve of instantaneous diffusion coefficient of mEos::HCN2 and mEos::HCN2ΔCNBD upon optical and pharmacological stimulation, respectively (n=16, mean± s.e.m from 2 biological replicates, ***p<0.001, 2-way Anova). **G, H)** Ratio of D_m and average fold change in D_m after pharmacological stimulation of HCN2, HCN2ΔCNBD and the HCN2 point mutants R591A and R591E (n=13, mean± s.e.m from 2 biological replicates, *p<0.05, **p<0.01, Mann-Whitney test). The mobility of mEos::HCN2 was significantly reduced on elevating intracellular cAMP levels by optical or pharmacological stimulation. On the contrary, the diffusion dynamics of HCN2ΔCNBD, HCN2 R591A and HCN2 R591E displayed slight alteration in presence of elevated cAMP. ns-not significant.

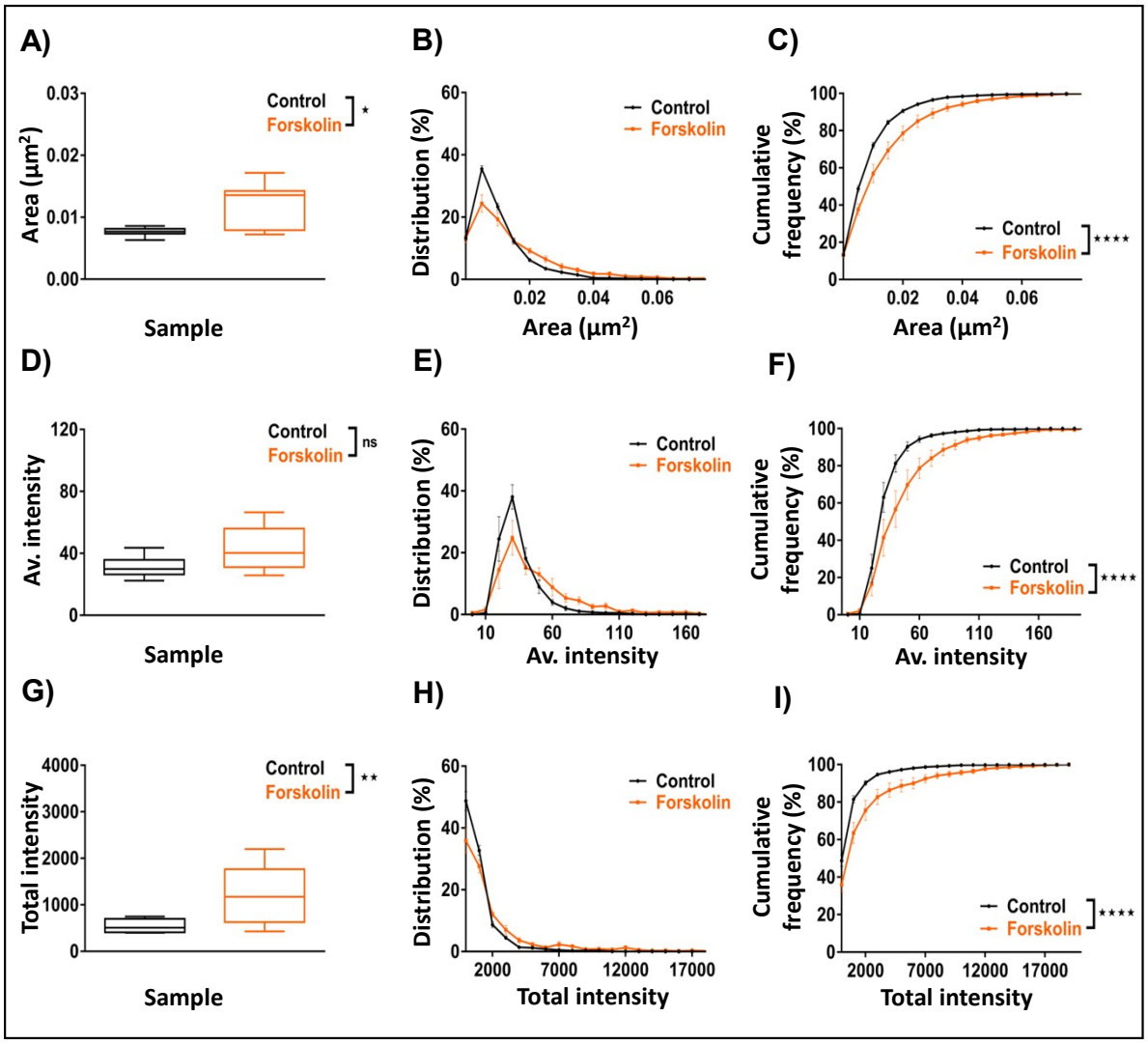

Figure S7. Morphological characteristics of nanoscale aggregation of ectopically expressed HCN2 after cAMP modulation by pharmacological application. A, D, G) Comparative analysis of area, average and total intensity of mEos::HCN2 clusters in control and forskolin treated cells, respectively (n=8, Median/IQR, *p<0.05, **p<0.01, Mann-Whitney test). **B, E, H)** Probability distributions of cluster area, average and total intensity of mEos::HCN2 clusters in control and forskolin treated cells, respectively. **C, F, I)** Cumulative frequency distributions of area, average and total intensity of mEos::HCN2 clusters in control and forskolin treated conditions, respectively (n=8, mean± s.e.m from 2 biological replicates, ****p<0.0001, 2-way Anova). An increase in the area and intensity of ectopically expressed mEos::HCN2 nanodomains was observed after pharmacological stimulation, compared to the control. ns-not significant.

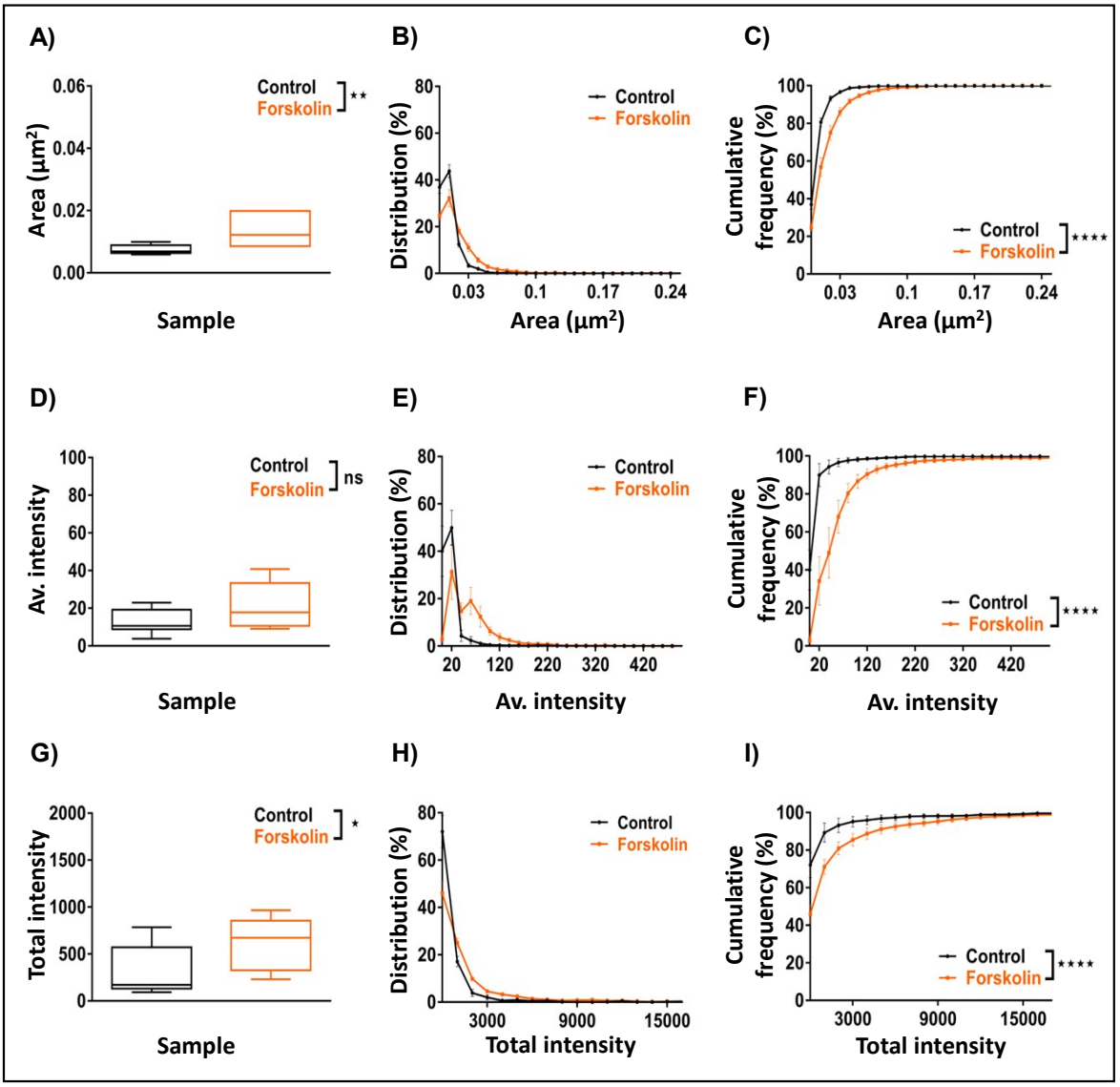

Figure S8. Morphological characteristics of nanoscale aggregation of endogenous HCN2 after cAMP modulation by pharmacological application. A, D, G) Comparative analysis of area, average and total intensity of endogenous HCN2 clusters in control and forskolin treated cells, respectively. (n=10, Median/IOR, *p<0.05, **p<0.01, Mann-Whitney test). **B, E, H)** Probability distributions of cluster area, average and total intensity of endogenous HCN2 clusters in control and forskolin treated cells, respectively. **C, F, I)** Cumulative frequency distributions of area, average and total intensity of endogenous HCN2 clusters in control and forskolin treated cells, respectively (n=10, mean± s.e.m from 2 biological replicates, ****p<0.0001, 2-way Anova). Similar to ectopically expressed HCN2, an increase in the area and intensity of endogenous HCN2 nanodomains was observed after pharmacological stimulation, compared to the control. ns-not significant.

	Parameters	bPAC-Flamindo	TpPAC-Flamindo	NgPAC1-Flamindo	NgPAC3-Flamindo
bPAC-Flamindo	Av.fold change in Intensity	-	ns	ns	ns
	Average lifetime	-	ns	***	ns
TpPAC-Flamindo	Av.fold change in Intensity	ns	-	ns	ns
	Average lifetime	ns	-	***	ns
NgPAC1-Flamindo	Av.fold change in Intensity	ns	ns	-	ns
	Average lifetime	***	***	-	***
NgPAC3-Flamindo	Av.fold change in Intensity	ns	ns	ns	-
	Average lifetime	ns	ns	***	-

Table S1: Statistical analyses of photodynamics of the PAC variants upon optogenetic activation.
The table illustrates the statistical significance for average fold change in intensity (Fig. 1C) and average lifetime (τ_{av}, Fig. 1D and E) between the different PACs-Flamindo (bPAC, TpPAC, NgPAC1 and NgPAC3). The asterisks indicate statistical significance (*** = p<0.001, ns=not significant). Photoactivation using 405 nm revealed slowest decay kinetics for NgPAC1 and fastest kinetics for TpPAC.

	Parameters	HCN2+bPAC	HCN2+TpPAC	HCN2+NgPAC1
HCN2+bPAC	τ	-	ns	***
	D_m	-	ns	ns
	Log D_m	-	**	****
	MSD	-	ns	****
	Area (nanodomain)	-	ns	ns
	Av. Intensity (nanodomain)	-	ns	ns
	Total Intensity (nanodomain)	-	ns	ns
HCN2+TpPAC	τ	ns	-	**
	D_m	ns	-	ns
	Log D_m	**	-	****
	MSD	ns	-	****
	Area (nanodomain)	ns	-	ns
	Av. Intensity (nanodomain)	ns	-	ns
	Total Intensity (nanodomain)	ns	-	ns
HCN2+NgPAC1	τ	***	**	-
	D_m	ns	ns	-
	Log D_m	****	****	-
	MSD	****	****	-
	Area (nanodomain)	ns	ns	-
	Av. Intensity (nanodomain)	ns	ns	-
	Total Intensity (nanodomain)	ns	ns	-

Table S2: Statistical analyses of photodynamics of mEos::HCN2 upon optogenetic activation of the PAC variants.
The table represents the statistical significance for mobility parameters of mEos::HCN2 upon photoactivation by different PACs (bPAC, TpPAC and NgPAC1). The parameters include the decay time constant (τ, Fig. 2D), instantaneous diffusion coefficient (D_m, Fig. 3B), Cumulative frequency of instantaneous diffusion coefficient (Fig. 3C), Mean square displacement (MSD, Fig. 3D), Area, Average Intensity and Total intensity of nanodomains (Fig. 4B-J). The asterisks indicate statistical significance (** =p<0.01, *** = p<0.001, **** = p<0.0001, ns=not significant). Between the PACs, targeted photoactivation of NgPAC1 alone showed a significant difference in the average lifetime of HCN2 diffusion. Similarly, a significant decrease in the MSD and shift in cumulative frequency of instantaneous diffusion coefficient of mEos::HCN2 was observed upon photoactivation of NgPAC1 compared to the other PACs, though there was no significant difference between the instantaneous diffusion coefficient (D_m) of mEos::HCN2 after photoactivation by the different PACs. Between the PAC variants, the morphological characteristics of the HCN2 nanodomains remained similar upon photoactivation.